

PCCP

Accepted Manuscript



This is an *Accepted Manuscript*, which has been through the Royal Society of Chemistry peer review process and has been accepted for publication.

Accepted Manuscripts are published online shortly after acceptance, before technical editing, formatting and proof reading. Using this free service, authors can make their results available to the community, in citable form, before we publish the edited article. We will replace this *Accepted Manuscript* with the edited and formatted *Advance Article* as soon as it is available.

You can find more information about *Accepted Manuscripts* in the [Information for Authors](#).

Please note that technical editing may introduce minor changes to the text and/or graphics, which may alter content. The journal's standard [Terms & Conditions](#) and the [Ethical guidelines](#) still apply. In no event shall the Royal Society of Chemistry be held responsible for any errors or omissions in this *Accepted Manuscript* or any consequences arising from the use of any information it contains.

Enabling electrochemical reduction of nitrogen to ammonia at ambient conditions through rational catalyst design[†]

Cite this: DOI: 10.1039/x0xx00000x

Received 00th January 2012,
Accepted 00th January 2012

DOI: 10.1039/x0xx00000x

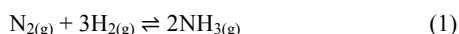
www.rsc.org/

Younes Abghoui^a, Anna L. Garden^a, Valtýr F. Hlynsson^a, Snædís Björgvinsdóttir^a, Hrefna Ólafsdóttir^a, Egill Skúlason^a

Commercial design of a sustainable route for on-site production of ammonia represents a potential economic and environmental breakthrough. In an analogous process to the naturally occurring enzymatic mechanism, synthesis of ammonia could be achieved in an electrochemical cell, in which electricity would be used to reduce atmospheric nitrogen and water into ammonia at ambient conditions. To date, such a process has not been realized due to slow kinetics and low faradaic efficiencies. Although progress has been made in this regard, at present there exists no device that can produce ammonia efficiently from air and water at room temperature and ambient pressure. In this work, a scheme is presented in which electronic structure calculations are used to screen for catalysts that are stable, active and selective towards N₂ electro-reduction to ammonia, while at the same time suppressing the competing H₂ evolution reaction. The scheme is applied to transition metal nitride catalysts. The most promising candidates are the (100) facets of the rocksalt structures of VN and ZrN, which show promise of producing ammonia in high yield at low onset potentials.

Introduction

Ammonia (NH₃) is one of the most highly produced chemicals worldwide and is primarily used in production of fertilizer^{1,2}. Ammonia is also gaining attention as an energy carrier and a potential transportation fuel due to its high energy density and lack of CO₂ emissions³. For the last century, ammonia has been synthesized primarily *via* the energy and capital intensive Haber-Bosch process in which gaseous nitrogen and hydrogen are passed over a Ru- or Fe-based catalyst at high pressure (150-350 atm) and high temperature (350-550 °C) to form NH₃ according to:^{4,5}



The H₂(g) for this process often comes from either coal or natural gas, both of which lead to increased production of various greenhouse gases. The alternative is to produce hydrogen from water splitting, which is a cleaner but very energy intensive process.

The Haber-Bosch process is in stark contrast to the function of the enzyme nitrogenase in bacteria in which ammonia is produced from solvated protons, electrons and atmospheric nitrogen at ambient conditions. The active site of the enzyme is a MoFe₇S₉N cluster that catalyses the electrochemical reaction:



The source of energy for this reaction is at least 16 adenosine triphosphate (ATP) molecules^{6,7}, which are used to increase the chemical potential of the electrons and the protons. It is thus an alluring prospect that this natural process could be emulated in a man-made, commercial installation. Instead of a separate H₂(g) production process, the protons could come from an acidic solution while the electrons would be driven to the electrode surface by an applied electric potential.

Various potential routes for ammonia synthesis at ambient conditions are currently being explored (see Refs. 1,2 and 8 for recent reviews). Numerous efforts have been made towards artificial synthesis of ammonia using photocatalytic⁹ and electrochemical¹⁰⁻¹⁵ methods. However, for many of these, it is difficult to regenerate the active nitrogen-fixing complex and only low current efficiencies (CE) (0.1~8 % at ambient conditions) have been obtained. To gain higher yields of ammonia, solid-state proton conductors have been employed, resulting in up to 78 % conversion of cathodic supplied nitrogen to ammonia^{16,17}. Ionic liquids or molten salts also promote

^a Science Institute and Faculty of Physical Sciences, VR-III, University of Iceland, IS-107 Reykjavik, Iceland.

[†] Electronic Supplementary Information (ESI) available: [Total energy of slabs for different facets, Free energy diagrams, corrections to the free energies, decomposition potentials and summary table are added for Results and discussion section]. See DOI: 10.1039/b000000x/

ammonia formation from low CE up to 72 % at high temperatures^{18–20}. While having achieved low-pressure ammonia synthesis, the abovementioned studies still suffer from the requirement of relatively high temperatures, which leads to increased product decomposition. Another drawback is the use of complex and expensive electrolytes that hinder commercialization. To the best of the authors' knowledge, the first observations of ammonia synthesis at milder conditions were reported with homogeneous catalysts with tungsten²¹ zirconium²² and tantalum²³ as the central atoms. However, for the sake of distributed use of ammonia, simpler methods are needed, ideally using heterogeneous catalysis, which allows for facile isolation of product.

In the past several years, numerous investigations have been conducted using various electrolytes and electrode materials to alleviate the thermodynamic requirements and optimize the ammonia formation rate using heterogeneous catalysis^{2,24–29}. Much research has been focused on electrolytic cells based on solid-state electrolytes and polymer electrolyte membranes (PEM). In such setups it is easier to separate the ammonia product from hydrogen feed gas and therefore to achieve considerable formation yield of ammonia. The highest rate of ammonia formation reported with Nafion membrane is $1.13 \times 10^{-8} \text{ mol s}^{-1} \text{ cm}^{-2}$ with a faradaic efficiency (FE) of ~90 % obtained at 80 °C where $\text{SmFe}_{0.7}\text{Cu}_{0.3-x}\text{Ni}_x\text{O}_3$ ($X = 0-0.3$) was used as the cathode³⁰. NH_4^+ was detected in dilute H_2SO_4 with pH of 3.85. This was obtained using wet H_2 as a feed gas. This is perhaps the reason for the improved formation rate of ammonia because water vapor may supply some protons³¹ and thus improve conductance and consequently enhance ammonia formation. Replacing the H_2 feed gas with water, electro-catalytic ammonia synthesis from N_2 and H_2O at room temperature was obtained at Ru cathode in a solid polymer electrolyte cell and 2M KOH³². Due to the hydrogen evolution reaction (HER) at the cathode, a low rate of ammonia formation ($3.4 \times 10^{-12} \text{ mol s}^{-1} \text{ cm}^{-2}$) with a low FE of 0.28 % was achieved at a relatively high potential (~ -1.3 V vs. SHE). The highest rate of ammonia synthesis that has been obtained thus far using air and water as feed gases is $1.14 \times 10^{-9} \text{ mol s}^{-1} \text{ cm}^{-2}$, achieved using a mixed NH_4^+/H^+ Nafion membrane³³. However, again a low FE (1 %) is observed and a high overpotential (-1.6 V) is necessary.

The above examples show that while solid state electrolytes or PEMs offer promise as an electrochemical route to ammonia formation, with production rates nearing that of commercial viability ($4.3 - 8.7 \times 10^{-7} \text{ mol s}^{-1} \text{ cm}^{-2}$)¹, they are still in the early stage of development and little is known of their stability. Furthermore, the manufacturing cost of the complicated electrolytes means that a simpler approach is desirable for realistic commercialization.

With advancements in the field of computations and modelling, theoretical investigations have provided deeper insight into catalysis^{34–47}, the importance of various active sites⁴⁸, and different mechanism of reactions^{49,50}. The use of computations can thus facilitate rational catalyst design, by enabling whole classes of material to be assessed for their suitability as catalysts. The simplest catalyst for electrochemical ammonia formation is a pure transition metal catalyst. In a recent theoretical study, electrochemical formation of ammonia on a range of flat and stepped transition metal surfaces was studied⁵¹. It was found that many metals require a relatively small overpotential of -0.5 to -1 V vs. SHE to form ammonia in 1 M aqueous electrolyte (pH = 0) at room temperature. However, the formation of $\text{H}_2(\text{g})$ can be very fast and severely hinder the production of ammonia unless the surface is covered with N-adatoms, rather than H-adatoms. It was found that the majority of metals are likely covered with H-adatoms at the onset potential of

ammonia formation. This is less likely for the early transition metals, however these are known to readily form oxides. Another study used a similar approach on transition metal nano-clusters⁴⁴ where molybdenum nano-clusters⁵² are reported to enhance the ammonia activity compared to HER. However, the presence of water in the electrochemical environment will reduce the efficiency of catalyst by blocking its active site due to preferential adsorption of oxygen rather than nitrogen⁵³.

In the present study, transition metal nitride catalysts are investigated for electrochemical formation of ammonia at ambient conditions. These materials offer the potential advantage of being able to form ammonia by way of a Mars-van Krevelen mechanism⁵⁴, in which a surface N atom is reduced to NH_3 and the catalyst later regenerated with gaseous N_2 , rather than adsorbing N_2 to the catalyst surface in the first step. Density functional theory (DFT) calculations are used to study the thermodynamics of the cathode reaction. Free energy diagrams are constructed for the electrochemical protonation of surface nitrogen or metal atoms to obtain onset potentials required for the ammonia synthesis on rocksalt and zincblende transition metal mononitride structures. The effect of an external potential is included by using the computational standard hydrogen electrode³⁴ and the lowest onset potential required to reduce N_2 to ammonia is estimated for each nitride. Poisoning of the catalyst, surface and defect stability and decomposition of the catalyst under an applied bias are also considered.

Methodology

DFT calculations

Mononitrides of all of the naturally occurring d-block metals are considered in the present study, in both the rocksalt (RS) and zincblende (ZB) structures. Two low index facets are considered for each crystal structure, the (100) and (111) facets of the RS structure and the (100) and (110) facets of the ZB structure. Each nitride surface is modelled by 40 atoms in five layers, with each layer consisting of four metal atoms and four nitrogen atoms. The bottom two layers are fixed whereas the top layers as well as the adsorbed species are allowed to relax. Boundary conditions are periodic in the x and y directions and surfaces are separated by 12 Å of vacuum in the z direction. The structural optimization is considered converged when the forces in any direction on all moveable atoms are less than 0.01 eV/Å. A previous study showed several of the 3d mononitrides to be either antiferromagnetic (RS VN, CrN, MnN, FeN and ZB MnN) or ferromagnetic (ZB VN, CrN) at their equilibrium lattice constants and as such are treated as spin-polarized⁵⁵. The RPBE lattice constants are also taken from that study.

The calculations are conducted with density functional theory (DFT) using the RPBE exchange correlation functional⁵⁶. A plane wave basis set with an energy cutoff of 350 eV is used to represent the valence electrons with a PAW⁵⁷ representation of the core electrons as implemented in the VASP code^{58–61}. Activation energies are calculated as the highest point along the minimum energy path (MEP) calculated using the climbing image nudged elastic band method (CI-NEB)^{62,63}. The self-consistent electron density is determined by iterative diagonalization of the Kohn-Sham Hamiltonian, with the occupation of the Kohn-Sham states being smeared according to a Fermi-Dirac distribution with a smearing parameter of $k_B T = 0.1$ eV. A $4 \times 4 \times 1$ Monkhorst-Pack k -point sampling is used for all the surfaces and maximum symmetry is applied to reduce the number of k -points in the calculations.

Electrochemical Reactions and Modelling

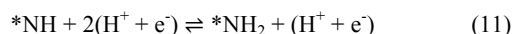
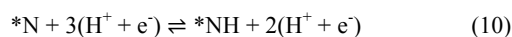
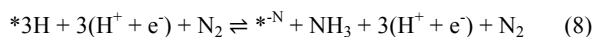
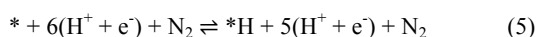
The cathode reaction of the electrochemical process is:



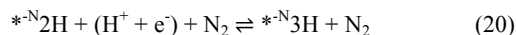
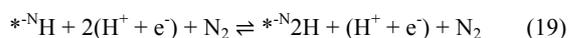
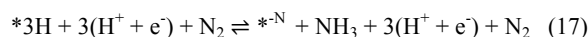
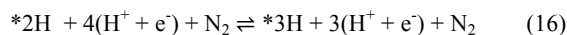
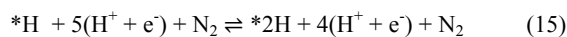
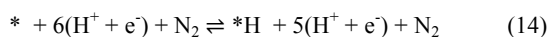
The source of protons is taken to be the anode reaction³⁴:



In this study a heterogeneous Mars-van Krevelen-type mechanism is considered where a surface N atom is reduced to NH₃ and the created nitrogen vacancy (N-vacancy) is then replenished with gaseous N₂. Hydrogenation of the surface is carried out by adding H atoms one-by-one to the surface to represent a proton from the solution and an electron from the electrode surface. The reaction mechanism is shown in Eqs. (5)-(13) and with ball-and-stick representation in Fig. 1.



An asterisk represents a site on the surface. A N-vacancy in the surface layer is denoted as *^N. DFT calculations are used to calculate the minimum energy configuration of each species on the surface and to calculate adsorption energies of all intermediates according to reactions (5)-(13). Various surface sites are considered and the optimal binding site is identified. A slightly different reaction mechanism is considered for the ZB surfaces and for RS ScN, TiN, CrN, YN and MnN, due to the existence of a prohibitively large thermochemical barrier to replenish the N-vacancy with gaseous N₂. In this mechanism, two NH₃ molecules are formed from two surface N atoms and a dimer N-vacancy is created before regenerating the catalyst with gaseous N₂. The mechanism is given in the Eqs. (14)-(22). In this mechanism, the barrier to fill the N-vacancy is greatly reduced and, in most cases, N₂ adsorption is no longer the rate-determining step (RDS).



As a first approximation when screening for catalytic activity, the surface site in Eqs. (5)-(13) or (14)-(22) is restricted to a single nitrogen site where each hydrogen (H⁺ + e⁻) is added to the same N atom. One NH₃ is formed after the addition of 3(H⁺ + e⁻) and the second NH₃ is formed after the addition of 6(H⁺ + e⁻) in total. This is hereafter referred to as a “constrained” mechanism. For a more detailed investigation of the catalytic activity this restriction is lifted and all possible adsorption sites for each proton are considered. This is accordingly referred to as an “unconstrained” mechanism. In this way, the possibility of a catalyst requiring more than six protons and electrons to form 2NH₃ is explored and also the possibility of forming H₂, rather than NH₃.

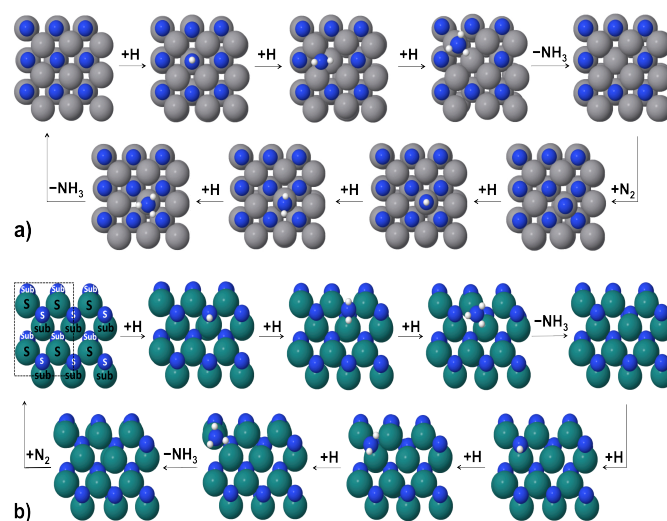


Fig. 1 Mars-van Krevelen mechanism for ammonia formation on the (100) facet of the RS structure (a) and the (110) facet of the ZB structure (b) of metal nitrides. For better illustration, more than one supercell is depicted but for the second ammonia molecule formation, the extra adsorbates that should be visible due to periodic boundary conditions are not shown. S stands for surface atoms and sub denotes the sub-layer.

It is assumed that activation barriers between stable minima can be neglected during the electrochemical reactions. The free energy of each elementary step is estimated at pH = 0 according to:

$$\Delta G = \Delta E + \Delta E_{\text{ZPE}} - T\Delta S \quad (23)$$

where ΔE is the reaction energy calculated using DFT. The zero-point energy correction (ΔE_{ZPE}) and entropy difference (ΔS) are calculated within a harmonic approximation and the values of these are given in supplementary material. The effect of an applied bias, U , is included for all electrochemical reaction steps by shifting the free energy for reactions involving n electrons by $-neU$:³⁴

$$\Delta G = \Delta E + \Delta E_{\text{ZPE}} - T\Delta S - neU \quad (24)$$

Explicit inclusion of a water layer⁶⁴ has not been considered in the present work due to the large computational effort required. It has been shown that the presence of water may help stabilize some species more than others via hydrogen bonding. For example, *NH is expected to be stabilized slightly by hydrogen bonding, while the

effect of the water layer on *N will be negligible. The effect of hydrogen-bond stabilization of the adsorbates has been estimated in a previous publication⁵¹. A relatively small correction for the N-H bonds was found of around 0.08 eV per H-bond. From this we conclude that the onset potentials calculated in the present study are likely to change by a similar magnitude, that is, less than 0.1 eV. Thus the correction is not done in the present study.

Results and Discussion

The computational screening process begins with 104 potential transition metal nitride catalysts. To assess the potential of each candidate for making NH₃ electrochemically at ambient conditions five considerations are investigated: (i) stability of the surface, (ii) stability of a surface N-vacancy, (iii) catalytic activity, (iv) poisoning of the catalyst surface and (v) an estimate of the electric potential needed to decompose the metal nitrides into its metal form and ammonia. These will be discussed in turn herein.

Stability of facets

As a first approximation in the search for a suitable catalyst, only the most stable crystal facet of the four facets considered in this study [RS(100), RS(111), ZB(100) and ZB(110)] is explicitly investigated for ammonia formation. Each slab is relaxed and the total energies compared to determine the most stable facet of a given metal nitride (see table. S1 in SI.). Most of the nitrides of the early transition metals (d¹⁻⁵) as well as the d⁹ metals are found to be most stable in the RS crystal structure and, for all of these, the (100) facet is more stable than the (111) facet. These are ScN, TiN, VN, CrN, MnN, YN, ZrN, NbN, MoN, HfN, TaN, CuN, and AgN. For most of the nitrides of the d⁶, d⁷ and d⁸ transition metals, the ZB (110) facet is the most stable. These are FeN, CoN, NiN, RuN, RhN, PdN, OsN, and IrN. These findings agree with the generally accepted trend of early transition metal nitrides being most stable in RS structure while the later transition metal nitrides are usually most stable in ZB⁶⁵⁻⁶⁷. Regarding facet stability, experimental studies show that the growth of films of ZrN, TiN, NbN and CrN results in the texture coefficient for the (100) planes of the synthesized polycrystalline to be one of the major preferential directions⁶⁸⁻⁷². For all considered surfaces of WN, ReN, AuN and PtN, significant distortion of the surface atoms is observed during relaxation and thus these nitrides are considered unstable and eliminated from further study. In total, this first consideration reduces the number of potential catalysts from 104 to 21. Among the candidates eliminated at this stage, it is of course possible that some structures/facets are also relatively stable and catalytically active. For simplicity the present work is restricted to only on the most stable facets and calculations for other facets are ongoing.

Stability of the surface nitrogen vacancy

In the Mars-van Krevelen mechanism considered in the present work, a surface nitrogen atom is reduced to form NH₃ after which the resulting vacancy is replenished by a gaseous N₂ molecule. For this replenishment to occur, the N-vacancy needs to be stable at the surface. If this is not the case, the N-vacancy may migrate to the bulk of the catalyst, that is, the reacted nitrogen on the surface is replaced with more nitrogen from the catalyst itself, rather than with gaseous N₂. This process can, in principle, continue until all the nitrogen atoms of the metal nitride have reacted and formed NH₃, leaving only the pure metal.

The stability of the N-vacancy at the surface of the catalyst is estimated by comparing the difference in energy of a nitride slab with a single N-vacancy in the surface layer ($E_{\text{vac},1}$) and to that of a single N-vacancy in the first subsurface layer ($E_{\text{vac},2}$). The minimum energy configuration of each of these slabs is found and the energy difference ($\Delta E_{\text{vac}} = E_{\text{vac},2} - E_{\text{vac},1}$) used as an estimation of the thermodynamic stability of the vacancy at the surface of the nitride. Activation barriers for vacancy migration ($E_{\text{a,vac}}$) are also calculated and both ΔE_{vac} and $E_{\text{a,vac}}$ are presented in Fig. 2. It is found that, for most of the nitrides, it is thermodynamically favourable for the vacancy to migrate to the bulk, with ΔE_{vac} less than or close to zero. However, it is clear that many of the nitrides exhibit a high activation barrier for vacancy migration and are thus likely to demonstrate a stable surface vacancy. All nitrides with an activation barrier for a vacancy migration of >1 eV are retained for further screening, since a barrier of such magnitude is unlikely to be overcome at room temperature.

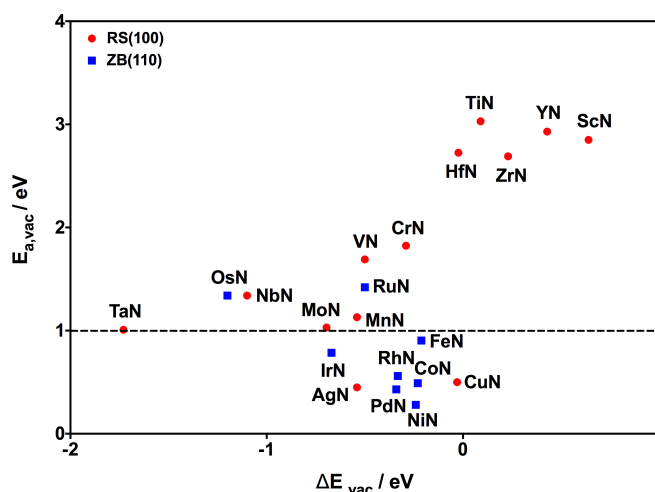


Fig. 2 Energy differences (ΔE_{vac}) of a vacancy at the surface layer and in the first subsurface layer of a nitride and the associated activation barrier of vacancy migration ($E_{\text{a,vac}}$). The dashed line at $E_{\text{a,vac}} = 1$ eV represents the cutoff above which metal nitrides are considered sufficiently stable for further study.

Catalytic activity

The catalytic activity of the nitrides towards electrochemical ammonia formation is initially calculated according to the constrained mechanism given in Eqs. (5)-(13) for most of the RS(100) nitride slabs and Eqs. (14)-(22) for all the ZB(110) nitrides and some of the RS(100) nitride slabs. The free energy of all intermediates is calculated according to Eq. 23, with reference to N₂ and H₂ in the gas phase. The free energy diagram for ZrN (RS) is presented in Fig. 3a where the effect of applied bias is included. Fig 3b shows the free energy diagram for MnN (RS), where the pathways towards NH₃ formation *via* both a single and a dimer vacancy are illustrated and compared.

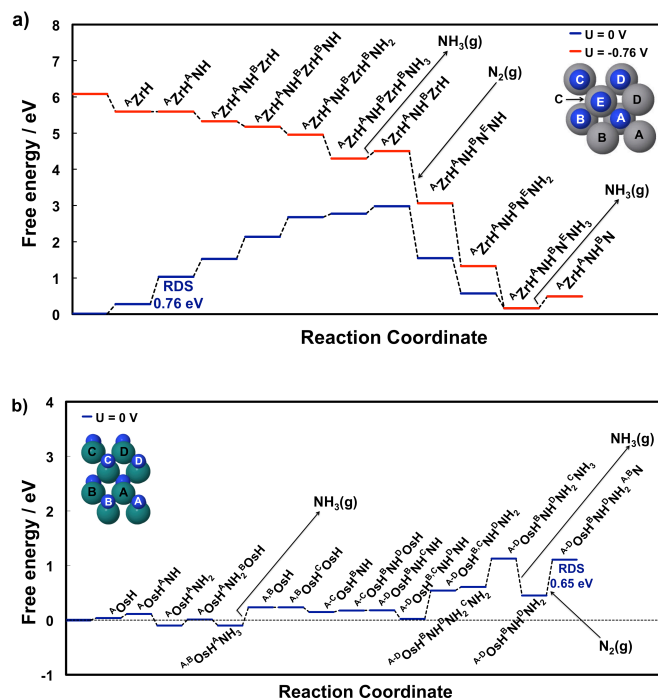


Fig. 5 Free energy diagram for NH_3 formation *via* an unconstrained Mars-van Krevelen mechanism on the (100) facet of RS ZrN (a) and the (110) facet of ZB OsN (b). For ZrN the rate-determining step is the second protonation step with $\Delta G = 0.76$ eV. Upon replenishment of the N-vacancy, one proton that was already adsorbed on Zr metal ($^{\text{B}}\text{ZrH}$) migrates to the N-atom to make NH ($^{\text{E}}\text{NH}$). The blue line indicates the free energy of all the stable intermediates calculated at zero potential. The red line represents the free energy of all the stable intermediates at the onset potential. For OsN the RDS is to fill the N-vacancy with $\Delta G = 0.65$ eV. As the RDS involves no proton-electron transfer, no bias is applied and the free energy landscape of OsN is depicted only at zero potential.

For VN, CrN and RuN, the mechanism is found to be identical to the constrained mechanism, where each added H adds to the same N atom, forming one NH_3 , then the second, with only $6(\text{H}^+ + \text{e}^-)$ required to form 2NH_3 . For ZrN, (Fig. 5a), allowing the H to bind to any surface site results in firstly a surface Zr atom being protonated, and then an N atom. The protonation of N is the RDS in NH_3 formation, similar to the constrained mechanism. However, the presence of an H atom on the adjacent Zr atom lowers the free energy of $^*\text{NH}$ formation by 0.23 eV. A similar case is seen for NbN, where two neighbouring Nb atoms are protonated before the RDS, which is protonation of the first surface N. The free energy of the RDS is lowered by 0.29 eV due to the H coverage on the Nb. For OsN and MnN the unconstrained mechanism leads to a different RDS and a different reaction path than when a constrained mechanism is considered. For MnN, $3(^*\text{NH}_2)$ and $1(^*\text{NH})$ form before the first ammonia is released and $9(\text{H}^+ + \text{e}^-)$ are needed to form 2NH_3 . In this case, no metal atoms are protonated. In contrast, for OsN, (Fig. 5b), H atoms cover all the metal atoms on the surface as well as surface N atoms and $13(\text{H}^+ + \text{e}^-)$ are needed to form 2NH_3 . For OsN addition of $\text{N}_{2(\text{g})}$ to fill the N-vacancy is endothermic, which corresponds to an increase in free energy that cannot be surpassed by an external applied bias as no proton-electron transfer is involved at this step.

An interesting trend that is observed from comparison of the constrained and unconstrained mechanisms is that for RS nitrides, a relatively low coverage of H is required to make 2NH_3 . Furthermore,

additional H atoms generally add to neighbouring metal atoms, rather than other N atoms, which lowers ΔG_{RDS} by $\sim 0.05 - 0.3$ eV, relative to the constrained mechanism. In contrast, for ZB nitrides, a higher coverage of H is needed to form 2NH_3 . The result of this is that ΔG_{RDS} is increased by ~ 0.12 eV, relative to the constrained mechanism. For such cases that require more than the minimum $6(\text{H}^+ + \text{e}^-)$ to form 2NH_3 , a lower faradaic efficiency is likely to be observed. For TiN and TaN an unconstrained mechanism yields a full H coverage on the surface with no NH_3 formation. The catalytic activity of these nitrides are thus instead being considered as potential hydrogen evolution catalysts, the results of which are beyond the scope of the present study.

After exclusion of those nitrides that either do not form NH_3 (TiN and TaN) or have an onset potential of >1.5 V (ScN, YN and HfN), eight metal nitride catalysts are considered potentially active towards NH_3 formation and presented in Fig. 6. The six RS nitrides as well as RuN ZB should make ammonia electrochemically under ambient conditions whereas ZB OsN likely requires high pressure to fill the N-vacancy in order to complete the catalytic cycle of ammonia formation.

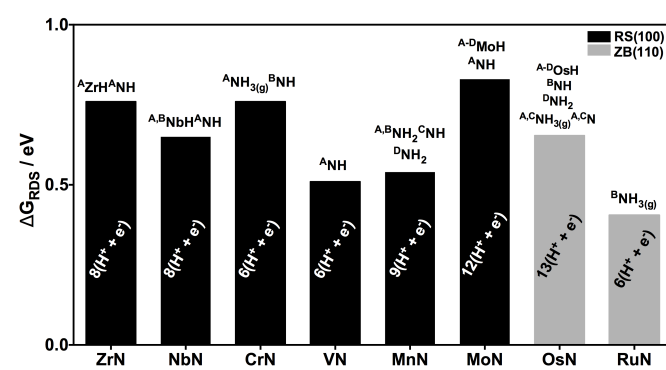


Fig. 6 Free energy change (ΔG_{RDS} , in eV) of the rate-determining step of NH_3 formation on transition metal nitride catalysts. An unconstrained mechanism is considered, where at each H addition step every possible adsorption site is investigated including other N atoms, metal atoms and bridging sites and at least $6(\text{H}^+ + \text{e}^-)$ are needed to form 2NH_3 . The labels above each bar indicate the species formed in the rate-determining step, the notation of which is explained in Fig. 5. The labels in each bar indicate the number of protons and electrons required to make 2NH_3 .

Poisoning of the surface vacancy

As previously discussed, in the Mars-van Krevelen mechanism considered in this work a surface N is reacted, leaving a surface vacancy at the surface and for the catalytic cycle to complete, this vacancy must be filled with $\text{N}_{2(\text{g})}$. However, there exists the possibility of the vacancy rather being filled with H atoms or O atoms from the aqueous electrolyte, both of which would block this surface site for completion of the catalytic cycle. In the present section the competition between N, O and H for filling the surface vacancy is investigated by considering the free energy of filling the vacancy with O or H relative to N ($\Delta G_{(*\text{N} \rightarrow \text{X})}$, where X = O or H). These free energies are referenced to N_2 , H_2O and H_2 in the gas phase and are calculated at the onset potential for each nitride. A negative value of $\Delta G_{(*\text{N} \rightarrow \text{X})}$ indicates that it is thermodynamically favourable to fill the vacancy with N, rather than O or H. The values of $\Delta G_{(*\text{N} \rightarrow \text{X})}$ are shown in Fig. 7 for all the catalytically active nitrides.

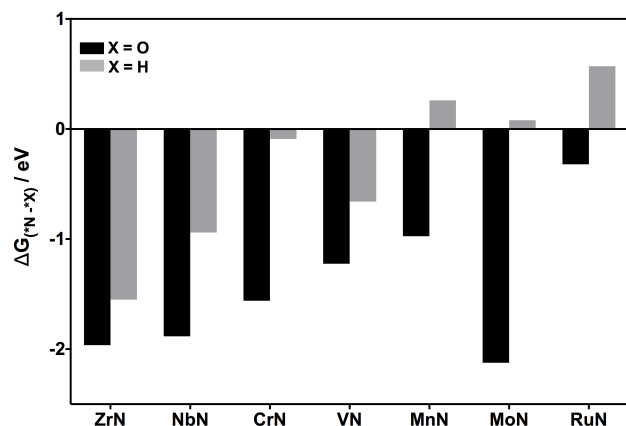
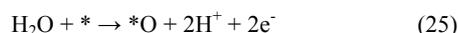


Fig. 7 Free energy of adsorption of O or H (relative to N) to the surface vacancy of catalytically active nitrides ($\Delta G_{(N-X)}$, in eV). Free energies are calculated relative to $N_{2(g)}$, $H_{2(g)}$ and $H_2O_{(g)}$. All free energies are evaluated at the calculated onset potential for each nitride: ZrN, -0.76 V; NbN, -0.65 V; CrN, -0.76 V; VN, -0.51 V; MnN, -0.54 V; MoN, -0.83 V; and RuN, -0.41.

It can be seen that N atoms bind more strongly to the surface vacancy than O atoms by over 1 eV for most nitrides. Thus it is unlikely that the surface vacancy will be poisoned by O atoms. For poisoning by H, however, it can be seen that the surface vacancy in MnN, MoN and RuN is likely to be filled by H, rather than N. For the remaining nitrides, ZrN, NbN, CrN and VN, the vacancy is likely refilled by N and thus the catalytic cycle may continue to form the second NH_3 . These results are as expected as when the bias is tuned towards more negative values, the electropositive O species bind weaker on the surface compared to H_2O in the gas phase, as they would rather form bonds with the surface when the bias is more positive:

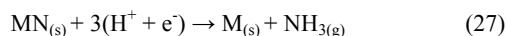


Conversely, the H adsorption free energy, becomes more negative when the bias is lowered:



Stability of the nitrides with respect to decomposition at onset potential

The final criterion considered in the present study for an appropriate metal nitride catalyst for electrochemical NH_3 formation is the stability of the catalyst with respect to decomposition when an external bias is applied. The decomposition of a metal mononitride (MN) into the corresponding pure metal (M) and NH_3 can be expressed as:



The overall free energy change of the reaction can be expressed in terms of free energies of formation as:

$$\Delta G_r = \Delta G_f(NH_{3(g)}) - \Delta G_f(MN_{(s)}) - 3\Delta G(H^+/e^-) \quad (28)$$

The term $3\Delta G(H^+/e^-)$ gives the contribution to the free energy by the protons and electrons. To find the applied potential at which the nitride is reduced to the metal, ΔG_r is required to be zero, or

$$3\Delta G(H^+/e^-) = \Delta G_f(NH_{3(g)}) - \Delta G_f(MN_{(s)}) \quad (29)$$

Therefore, the required potential can be expressed as:

$$U = -\Delta G(H^+/e^-)/3 \quad (30)$$

The free energy of formation of each nitride is calculated using DFT and the free energy of formation of $NH_{3(g)}$ is taken to be -0.17 eV at standard conditions⁷⁴. The decomposition potential of all the catalytically active nitrides are given in Fig. 8. For a given nitride to be suitable for electrochemical formation of NH_3 , the decomposition potential must be more negative than the onset potential for the ammonia formation.

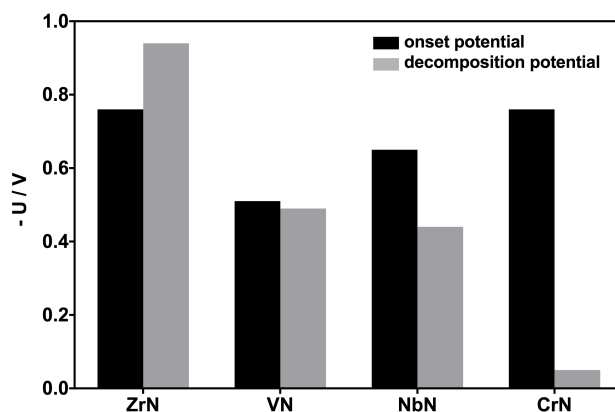


Fig. 8 Decomposition potential for stable and active metal nitrides according to Eq. 27. Also included are the calculated onset potentials for electrocatalytic NH_3 formation. All values are calculated at 300 K (see table 3 in ESI).

According to Fig. 8, ZrN is the only candidate that should not decompose at the electric potential needed to form ammonia. However, it should be emphasized that this is a purely thermodynamic analysis and no kinetic effects are taken into account. As was seen earlier in Section 3.2 (Fig 2), activation barriers for the first step of decomposition of the metal nitride into the metal and ammonia usually involves high activation barriers (between 1 and 3 eV), which would mean that although thermodynamically unstable, decomposition of most nitrides would be extremely slow at room temperature. For VN, the onset potential is similar as the potential required to decompose the nitride. However, the activation barrier for the N-vacancy to migrate into the bulk is around 1.7 eV and so the nitride might be maintained by replenishing the N-vacancies with $N_{2(g)}$. Given the standard error in DFT and in our models applied here, and the relatively high barrier to N-vacancy migration (1.34 eV), NbN may perhaps be used as a catalyst too. For CrN, the decomposition potential is much less negative than the onset potential and this will likely decompose before appreciable amounts of NH_3 will be formed. (See Table 4 in ESI for summary).

The culmination of the five criteria investigated in this screening for a potential electro-catalyst for electrochemical ammonia formation at ambient conditions yields two very promising candidates, namely ZrN and VN (both RS(100)). ZrN is particularly promising as it has been shown experimentally that RS is the most stable ground-state configuration⁷⁵, and the (100) is always one of the preferential texture coefficients^{68,69,72,76}. In contrast to pure transition metals⁵¹, the surface of these nitride catalysts are not likely to get covered by hydrogen at the onset potentials required for ammonia formation. As a result, faradaic losses due to the competitive HER, which is the main limiting issue with pure transition metals⁵¹, should not occur

for these nitrides. Hence, high yield of ammonia formation is predicted in experiments. Furthermore, the catalysts require only a low applied bias for ammonia formation and are likely stable towards poisoning and decomposition.

Summary and Conclusions

In this paper, an efficient scheme is proposed that utilizes first principles calculations to screen for nitrogen reduction electrocatalysts that efficiently form ammonia at ambient conditions and in aqueous electrolyte. In this work the scheme is applied to transition metal nitrides. However, it could also be utilized for any reaction where the possibility of Mars-van Krevelen mechanism is explored. The most promising nitride catalysts are the (100) facets of rocksalt VN and ZrN, which should form ammonia at -0.51 V and -0.76 V with respect to SHE, respectively. The suggested catalysts should not decompose or be poisoned by oxygen or hydrogen from the aqueous electrolyte. NbN could also be a good catalyst worthy of further investigations if kinetic barriers are sufficiently high as to avoid decomposition with an applied bias. In contrast to previous studies where relatively high onset potentials are required for ammonia formation and hydrogen evolution is a competing reaction^{51,52}, the most promising RS candidates presented in this paper (VN and ZrN) only need a low applied bias to form ammonia and the competing HER is suppressed. Therefore, a significant amount of ammonia compared with hydrogen gas can be expected. Furthermore, at the onset potential, the N-vacancy is stable towards both protonation and oxidation from water and it should get easily repaired with atmospheric nitrogen injected to the system at ambient conditions. Other crystal facets and other mechanisms of ammonia formation on these nitride catalysts are currently being studied to further investigate the catalytic capability of this class of catalyst. Experimentalists are strongly encouraged to test these promising candidates for the possibility of high yield electrochemical ammonia production at ambient conditions.

Acknowledgements

The authors would like to thank Prof. Tejs Vegge, Prof. Ib Chorkendorff and Dr. Jakob G. Howalt at the Technical University of Denmark (DTU) and Prof. Hannes Jónsson of the University of Iceland for helpful discussions. Financial support is acknowledged from the Icelandic Research Fund, Nordic Energy Research by way of the Nordic Initiative for Solar Fuel Development, the Icelandic Student Innovation Fund, and the Research Fund of the University of Iceland. The calculations were in part carried out on the Nordic high performance computer (Gardar).

References

- S. Giddey, S. P. S. Badwal, and A. Kulkarni, *Int. J. Hydrogen Energy*, 2013, **38**, 14576–14594.
- I. A. Amar, R. Lan, C. T. G. Petit, and S. Tao, *J. Solid State Electrochem.*, 2011, **15**, 1845–1860.
- A. Klerke, C. H. Christensen, J. K. Nørskov, and T. Vegge, *J. Mater. Chem.*, 2008, **18**, 2304–2310.
- V. Smil, *Sci. Am.*, 1997, **277**, 76–81.
- J. R. Jennings, *Catalytic ammonia synthesis: fundamentals and practice*, Plenum, New York, 1991.
- J. M. Berg, J. L. Tymoczko, and L. Stryer, *Biochemistry*, W. H. Freeman, New York, 2002.
- B. K. Burgess and D. J. Lowe, *Chem. Rev.*, 1996, **96**, 2983–3012.
- I. Garagounis, V. Kyriakou, A. Skodra, E. Vasileiou, and M. Stoukides, *Front. Energy Res.*, 2014, **2**, 1–10.
- T. D. Schrauzer, N. Guth, *J. Am. Chem. Soc.*, 1977, **99**, 7189–7193.
- J. Y. Becker, *J. Electroanal. Chem. Interfacial Electrochem.*, 1988, **250**, 385–397.
- J. Y. Becker and S. A. Tsarfaty, *J. Electroanal. Chem. Interfacial Electrochem.*, 1990, **280**, 119–127.
- C. Pickett and J. Talarmin, *Nature*, 1985, **317**, 652–653.
- A. Sclafani, V. Augugliaro, and M. Schiavello, *J. Electrochem. Soc.*, 1983, **130**, 734–736.
- D. V. Yandulov and R. R. Schrock, *Science*, 2003, **301**, 76–78.
- N. Furuya and H. Yoshida, *J. Electroanal. Chem. Interfacial Electrochem.*, 1990, **291**, 269–272.
- G. Marnellos and M. Stoukides, *Science*, 1998, **282**, 98–100.
- G. Marnellos, S. Zisekas, and M. Stoukides, *J. Catal.*, 2000, **193**, 80–87.
- T. Murakami, T. Nishikiori, T. Nohira, and Y. Ito, *J. Am. Chem. Soc.*, 2003, **125**, 334–335.
- T. Murakami, T. Nohira, T. Goto, Y. H. Ogata, and Y. Ito, *Electrochim. Acta*, 2005, **50**, 5423–5426.
- T. Murakami, T. Nohira, Y. Araki, T. Goto, R. Hagiwara, and Y. H. Ogata, *Electrochem. Solid-State Lett.*, 2007, **10**, E4–E6.
- J. Catt, A. J. Pearman, and R. L. Richards, *Nature*, 1975, **253**, 39–40.
- J. Pool, E. Lobkovsky, and P. Chirik, *Nature*, 2004, **427**, 527–530.
- P. Avenier, M. Taoufik, A. Lesage, X. Solans-Monfort, A. Baudouin, A. de Mallmann, L. Veyre, J.-M. Basset, O. Eisenstein, L. Emsley, and E. A. Quadrelli, *Science*, 2007, **317**, 1056–1060.
- A. Denvir and O. Murphy, *US Patent*, US7314544 B2, 2008.
- M. Ouzounidou, A. Skodra, C. Kokkofitis, and M. Stoukides, *Solid State Ionics*, 2007, **178**, 153–159.
- T. M. Pappenfus, K. Lee, L. M. Thoma, and C. R. Dukart, *ECS Trans.*, 2009, **16**, 89–93.
- I. A. Amar, R. Lan, C. T. G. Petit, V. Arrighi, and S. Tao, *Solid State Ionics*, 2011, **182**, 133–138.
- B. Lin and K. Wei, *Catal. Commun.*, 2013, **41**, 110–114.
- Z. Song, T. Cai, J. C. Hanson, J. A. Rodriguez, and J. Hrbek, *J. Am. Chem. Soc.*, 2004, **126**, 8576–8584.
- G. Xu, R. Liu, and J. Wang, *Sci. China Ser. B Chem.*, 2009, **52**, 1171–1175.
- Z. J. Li, J. D. Wang, R. Q. Liu, Y. H. Xie, *J. Chin Rare Earth Soc.*, 2005, **23**, 62–67.
- V. Kordali, G. Kyriacou, and C. Lambrou, *Chem. Commun.*, 2000, 1673–1674.
- R. Lan, J. T. S. Irvine, and S. Tao, *Sci. Rep.*, 2013, **3**, 1–7.
- J. K. Nørskov, J. Rossmeisl, A. Logadottir, L. Lindqvist, J. R. Kitchin, T. Bligaard, and H. Jónsson, *J. Phys. Chem. B*, 2004, **108**, 17886–17892.
- J. Greeley and M. Mavrikakis, *Nat. Mater.*, 2004, **3**, 810–815.
- K. Honkala, A. Hellman, I. N. Remediakis, A. Logadottir, A. Carlsson, S. Dahl, C. H. Christensen, and J. K. Nørskov, *Science*, 2005, **307**, 555–558.
- J. Hafner and C. Wolverton, *MRS Bull.*, 2006, **31**, 659–668.
- F. Abild-Pedersen, J. Greeley, F. Studt, J. Rossmeisl, T. Muntzer, P. Moses, E. Skúlason, T. Bligaard, and J. Nørskov, *Phys. Rev. Lett.*, 2007, **99**, 0161051–0161054.
- F. Studt, F. Abild-Pedersen, T. Bligaard, R. Z. Sørensen, C. H. Christensen, and J. K. Nørskov, *Science*, 2008, **320**, 1320–1322.
- H.-J. Freund and G. Pacchioni, *Chem. Soc. Rev.*, 2008, **37**, 2224–2242.
- J. Greeley, I. E. L. Stephens, A. S. Bondarenko, T. P. Johansson, H. A. Hansen, T. F. Jaramillo, J. Rossmeisl, I. Chorkendorff, and J. K. Nørskov, *Nat. Chem.*, 2009, **1**, 552–556.
- J. K. Nørskov, T. Bligaard, J. Rossmeisl, and C. H. Christensen, *Nat. Chem.*, 2009, **1**, 37–46.
- J. K. Nørskov, F. Abild-Pedersen, F. Studt, and T. Bligaard, *Proc. Natl. Acad. Sci. U. S. A.*, 2011, **108**, 937–943.
- J. G. Howalt, T. Bligaard, J. Rossmeisl, and T. Vegge, *Phys. Chem. Chem. Phys.*, 2013, **15**, 7785–7795.
- V. Tripkovic, M. Vanin, M. Karamad, M. E. Björketun, K. W. Jacobsen, K. S. Thygesen, and J. Rossmeisl, *J. Phys. Chem. C*, 2013, **117**, 9187–9195.
- A. Verdaguier-Casadevall, D. Deiana, M. Karamad, S. Siahrostami, P. Malacrida, T. W. Hansen, J. Rossmeisl, I. Chorkendorff, and I. E. L. Stephens, *Nano Lett.*, 2014, **14**, 1603–1608.

47. A. A. Peterson, F. Abild-Pedersen, F. Studt, J. Rossmeisl, and J. K. Nørskov, *Energy Environ. Sci.*, 2010, **3**, 1311–1315.
48. S. Dahl, A. Logadottir, R. Egeberg, J. Larsen, I. Chorkendorff, E. Törnqvist, and J. Nørskov, *Phys. Rev. Lett.*, 1999, **83**, 1814–1817.
49. S. Gudmundsdóttir, E. Skúlason, and H. Jónsson, *Phys. Rev. Lett.*, 2012, **108**, 156101–156105.
50. S. Kattel, P. Atanassov, and B. Kiefer, *Phys. Chem. Chem. Phys.*, 2013, **15**, 148–153.
51. E. Skúlason, T. Bligaard, S. Gudmundsdóttir, F. Studt, J. Rossmeisl, F. Abild-Pedersen, T. Vegge, H. Jónsson, and J. K. Nørskov, *Phys. Chem. Chem. Phys.*, 2012, **14**, 1235–1245.
52. J. G. Howalt and T. Vegge, *Phys. Chem. Chem. Phys.*, 2013, **15**, 20957–20965.
53. J. Howalt and T. Vegge, *Beilstein J. Nanotechnol.*, 2014, **5**, 111–120.
54. P. Mars and D. W. Van Krevelen, *Eng. Sci.*, 1954, **3**, 41–45.
55. V. F. Hlynsson, E. Skúlason, and A. L. Garden, *J. Alloys Compd.*, 2014, **603**, 172–179.
56. B. Hammer, L. Hansen, and J. Nørskov, *Phys. Rev. B*, 1999, **59**, 7413–7421.
57. P. Blöchl, *Phys. Rev. B*, 1994, **50**, 17953–17979.
58. G. Kresse and J. Hafner, *Phys. Rev. B*, 1993, **47**, 558–561.
59. G. Kresse and J. Hafner, *Phys. Rev. B*, 1994, **49**, 14251–14269.
60. G. Kresse and J. Furthmüller, *Comput. Mater. Sci.*, 1996, **6**, 15–50.
61. G. Kresse and J. Furthmüller, *Phys. Rev. B. Condens. Matter*, 1996, **54**, 11169–11186.
62. G. Henkelman, B. P. Uberuaga, and H. Jónsson, *J. Chem. Phys.*, 2000, **113**, 9901–9904.
63. G. Henkelman and H. Jónsson, *J. Chem. Phys.*, 2000, **113**, 9978–9985.
64. E. Skúlason, V. Tripkovic, M. E. Björketun, S. Gudmundsdóttir, G. Karlberg, J. Rossmeisl, T. Bligaard, H. Jónsson, and J. K. Nørskov, *J. Phys. Chem. C*, 2010, **114**, 18182–18197.
65. B. Eck, R. Dronskowski, M. Takahashi, and S. Kikkawa, *J. Mater. Chem.*, 1999, **9**, 1527–1537.
66. C. Stampfl, W. Mannstadt, R. Asahi, and A. Freeman, *Phys. Rev. B*, 2001, **63**, 1551061–15510611.
67. S. K. R. Patil, N. S. Mangale, S. V. Khare, and S. Marsillac, *Thin Solid Films*, 2008, **517**, 824–827.
68. H. J. Ramos and N. B. Valmorla, *Vacuum*, 2004, **73**, 549–554.
69. D. F. Arias, Y. C. Arango, and a. Devia, *Appl. Surf. Sci.*, 2006, **253**, 1683–1690.
70. P. Hones, R. Sanjines, and F. Levy, *Surf. Coatings Technol.*, 1997, **94**, 398–402.
71. S. Shayestehaminzadeh, T. K. Tryggvason, F. Magnus, S. Olafsson, and J. T. Gudmundsson, *Thin Solid Films*, 2013, **549**, 199–203.
72. E. Gillan and R. Kaner, *Inorg. Chem.*, 1994, **768**, 5693–5700.
73. R. Michalsky, Y.-J. Zhang, A. J. Medford, and A. A. Peterson, *J. Phys. Chem. C*, 2014, **118**, 13026–13034.
74. D. R. Lide, *CRC Handbook of Chemistry and Physics*, Florida, 78th edn., 1997.
75. L. A. Salguero, L. Mancera, J. A. Rodríguez, and N. Takeuchi, *Phys. Status Solidi*, 2006, **243**, 1808–1812.
76. C. Ma, J. Huang, and H. Chen, *Surf. Coatings Technol.*, 2000, **134**, 289–294.